APPLICATION OF A TWO-STAGE ALGORITHM FOR ADAPTIVE DETECTION IN HYPERSPECTRAL IMAGING

Michael D. Farrell Jr. and Russell M. Mersereau

Center for Signal & Image Processing
School of Electrical & Computer Engineering
Georgia Institute of Technology
Atlanta, GA 30332
{mfarrell, rmm}@ece.gatech.edu

ABSTRACT

Adaptive detection has a rich history in the radar community, and a number of other areas have borrowed heavily from constructs developed in this field. The task of target detection in hyperspectral imaging (HSI) is one such area that has recently begun to take advantage of parallels from the field of radar array processing. While there are key differences between the physical setup and data collected by radar and hyperspectral systems, the formulation of the adaptive detection problem is remarkably similar. In this paper we apply a two-stage detection approach originally developed for STAP in airborne radar to adaptive target detection in hyperspectral imaging. Touching first on the component algorithms involved, and then on their similarities and differences, we show that this two-stage approach has an interesting conceptual interpretation for HSI that comes from the multi-dimensional Euclidean geometry of the spectral measurement space. However, due to the nature of hyperspectral target signatures and background statistics, we propose that there are many scenarios where HSI detection may be better served by reversing the order of stages applied to the data as laid out in previous formulations. Detection results for ground targets are presented to illustrate the potential of this new two-stage approach in hyperspectral adaptive detection.

1. INTRODUCTION

The most common formulation of the adaptive detection problem harkens back to the work of [1]. In the decade of the 1980's this framework was utilized and extended in algorithm development for contemporary airborne radar systems whose capabilities were advancing. Kelly, Fuhrmann, and others made seminal contributions such as [2]. That paper espoused the Generalized Likelihood Ratio Test (GLRT) approach, which despite being sub-optimal, has become a trusted performance benchmark for practical situations where interference is assumed Gaussian and homogeneous.

Following the formulation of [1]-[2], we define the problem of adaptive detection as seeking signal (target) presence in a $L \times 1$ vector observation $\mathbf{x}$. This primary data vector is complex in the radar world and often called a *snapshot* in the literature, but in our case for hyperspectral imaging (HSI) this vector is real and is sometimes called the *pixel under test* (PUT). The sample $\mathbf{x}$ has a covariance matrix denoted by $\mathbf{\Gamma}$, which is assumed to be an unknown parameter.[1] It is desired to classify the primary data vector as one of two categories:

$$H_0 : \mathbf{x} = \mathbf{w}, \qquad \texttt{or} \qquad H_1 : \mathbf{x} = a\mathbf{s} + \mathbf{w}. \tag{1}$$

The primary data vector either consists of noise only under the H_0 hypothesis, or it consists of a signal plus noise under the H_1 hypothesis. When the target signal is present in $\mathbf{x}$, the array response vector (or spectral signature in the case of hyperspectral) is multiplied by an unknown but deterministic scalar signal parameter a. The fact that this detection problem has two unknowns, $\mathbf{\Gamma}$ and a, is what necessitates the use of so called 'adaptive' methods. Specifically, we require a secondary data set (i.e. training data) of N samples, which we denote $\mathbf{X} = [\mathbf{x}_1|\mathbf{x}_2|\dots|\mathbf{x}_N]$, that are independently and identically distributed (i.i.d.) and share the same covariance as the primary data vector. In order to ensure that the data covariance is invertible (i.e. non-singular), we assume that $N \geq L$. This is no problem for HSI, as typical values are $N = 200000$ and $L = 200$. Further, Gaussian statistics are assumed. As such, when the target is absent under H_0, $\mathbf{x} \sim N(\mathbf{0}, \mathbf{\Gamma})$, and when the target is present under H_1, $\mathbf{x} \sim N(a\mathbf{s}, \mathbf{\Gamma})$.

Funding support from the U.S. Army Research Office under contract number DAAD19-02-2-0012 is gratefully acknowledged for this work.

[1] Note that here we use the normalized sample covariance matrix (SCM), which differs from the analysis seen in some radar-focused publications. Using the unnormalized covariance matrix amounts to a scaling of the detection statistic and threshold by N.

In hyperspectral imaging, the PUT **x** is a spectrum characterizing the material on the ground within the pixel's spatial extent. In many STAP applications, the snapshot **x** is a range-Doppler-azimuth cell taken from the column of one range-gated slice of post-Doppler processed data.

2. ADAPTIVE SIDELOBE BLANKER

The adaptive sidelobe blanker (ASB) is an adaptive detection algorithm presented in [3] that consists of a two stage cascade. This algorithm was proposed to allay the large number of false alarms associated with various GLRT-type detectors in the presence of insufficiently nulled (e.g. inhomogeneous) interference for radar. For radar, the ASB detector is characterized in terms of mainbeam performance and sidelobe target rejection. The ASB consists of a first stage adaptive matched filter (AMF) [4] followed by a second stage adaptive coherence estimator (ACE) [5]. Only those samples that survive both detection thresholdings are declared target bearing. In this paper, we concern ourselves with the standard case where the data is homogeneous and there is no mismatch between the estimated data covariance and the variability actually present in each PUT[2]. For each radar snapshot tested, the AMF detector measures the power originating from the assumed target direction (in element space). The ACE detector determines what fraction of the total energy present in the snapshot originated form the target direction. Only snapshots surviving both thresholdings are declared target bearing, and essentially the ASB is a binary "and" of the AMF and ACE detectors. Figure 1 depicts an example of ASB decision regions, which, of course, are fluid with the placement of the two thresholds. Note the AMF is on the x-axis, which reinforces the fact that this statistic is computed first for all samples, and only those samples surviving AMF thresholding are put to the ACE. Rather than being a single point the ASB threshold is actually a pair of values, meaning that an iso-contour exists within the two-dimensional space that defines a range of values that will achieve an equivalent P_D. For more on novel thresholding approaches for the ASB, see [6].

In the next section, we look at how the two-stage ASB formulation relates to our goal of detecting targets using hyperspectral imaging sensors.

[2]In practice, this assumption can be violated due to training data that is poor, contaminated, or generally unrepresentative of operating conditions. In its full glory, the unrestricted case of $\hat{\mathbf{\Gamma}} \neq \mathbf{\Gamma}$ is quite difficult. But if the restriction of a 'generalized eigen relation' [7] is imposed there is still reasonable performance and closed-form analysis.

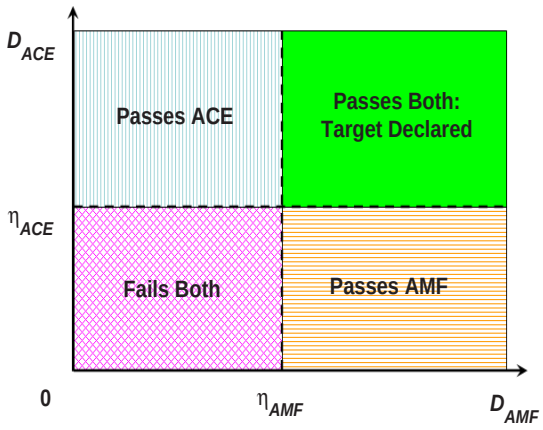

Fig. 1. Example of decision regions for ASB detector.

3. APPLICATION TO HYPERSPECTRAL IMAGING

Unlike monochromatic or standard RGB color imagery which have only one or three color planes, respectively, hyperspectral images are actually cubes formed from the stacking of hundreds of color planes simultaneously measured over the same spatial area. Hyperspectral data cubes seek to capture fine spectral features of the materials in the scene that are only discernable with data collected by sophisticated imaging spectrometers. Often, these sensors have more than 200 image channels, each capturing the energy in a narrow band of spectrum (typically $\sim$ 10nm in wavelength). For example, many HSI sensors are designed to cover the reflective portion of the electromagnetic spectrum – covering the visible, near infrared (NIR), and short-wave infrared (SWIR) – roughly 400 nm to 2500 nm. In target detection applications, many objects have unique reflective spectral properties that allow them to be identified despite their similarity to other objects in a morphological or RGB color perspective. For an introduction to HSI data exploitation, see [8] and other articles in that volume.

The analogy of spatial elements in a radar array to image channels in a hyperspectral sensor is the linchpin of applying existing approaches to our problem. Obviously, the systems themselves have a variety of differences – including the passive (HSI) vs. active (radar) nature of scene illumination, the real valued vs. complex valued signals, and the electrooptical phenomenology of hyperspectral sensing vs. the electromagnetic nature of radar.

When the AMF detector is considered for the hyperspectral case, it can be seen in figure 2 that this detector is concerned with the length of the pixel vector under test. It is measuring the amplitude (power) of the sample **x** and the threshold rejects samples that are not far enough away

from the collective interference[3]. The rank-one case of the AMF is

$$D_{AMF}(\mathbf{x}) = \frac{(\mathbf{s}^T\hat{\mathbf{\Gamma}}^{-1}\mathbf{x})^2}{(\mathbf{s}^T\hat{\mathbf{\Gamma}}^{-1}\mathbf{s})}. \quad (2)$$

The ACE detector, on the other hand, has a completely different geometrical interpretation. ACE sets an angular threshold and is concerned with the angle the test sample makes with our deterministic target template[4]. The angular threshold rejects pixels whose spectral angle is too large to be considered similar to the target signal. The rank-one case of the ACE is

$$D_{ACE}(\mathbf{x}) = \frac{(\mathbf{s}^T\hat{\mathbf{\Gamma}}^{-1}\mathbf{x})^2}{(\mathbf{s}^T\hat{\mathbf{\Gamma}}^{-1}\mathbf{s})(\mathbf{x}^T\hat{\mathbf{\Gamma}}^{-1}\mathbf{x})}. \quad (3)$$

In radar the data $\mathbf{X}$ is assumed zero-mean, and in order to accommodate this in hyperspectral processing, the mean of the background $\boldsymbol{\mu_0}$ is removed from all observations $\mathbf{x}_i$, pixels $i = 1, \ldots, N$.

Figure 2 illustrates the notion of different threshold interpretations for the components of the ASB detection algorithm. In two dimensions the AMF threshold is a line and the ACE threshold is a triangle. In three dimensions the AMF threshold is a plane orthogonal to the direction of the target signature from the origin of the interference, and the ACE threshold is a conic section beginning at the origin of the interference. When there is no signature information for a given target, the test is reduced to anomaly detection. In this case any pixels that are significantly spectrally different from the background will yield a high value. This is embodied by a certain separation from the center of the interference, and graphically the anomaly detection threshold is a sphere in three dimensions.

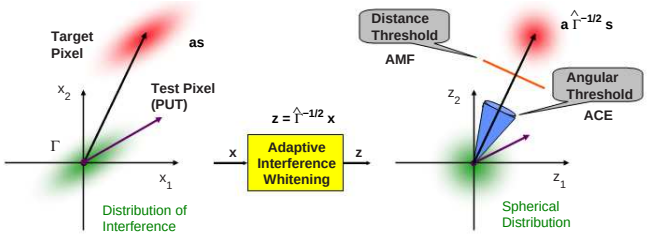

Fig. 2. Two dimensional illustration of the thresholds used.

[3]Background is a common term used in the remote sensing literature, however, interference is really more appropriate since it refers to clutter in the scene as well as sensor and atmospheric noise.

[4]There are full-rank versions of both detectors that can be used on targets that have both shape and amplitude variability. In that case, **S** is a matrix whose columns describe the uncertainty in the target and **a** becomes a vector. See [4],[5] for details.

4. ASB PERFORMANCE EVALUATION

The probability of detection (P_D) of this two-stage algorithm is the probability of a given PUT $\mathbf{x}$ yielding a point in the upper right section of figure 1. More precisely, the P_D is given by the probability of the outcome ($D_{AMF} > \eta_{AMF}, D_{ACE} > \eta_{ACE}$) when H_1 is true. This is

$$P_D = \Pr[D_{AMF} > \eta_{AMF}, D_{ACE} > \eta_{ACE}]. \quad (4)$$

Specifying the likelihood of this outcome cannot be done without knowing the distributions of D_{AMF} and D_{ACE} as well their dependence. Unfortunately, defining and explaining all the terms in the conditional and full probabilities that characterize P_D is beyond the length of this paper, and a thorough narrative for the terms and equations can be found in [9]. To meet length requirements, here we simply present the expressions leading to P_D for the ASB and refer to the reader to the citations for appropriate detail.

$$D_{AMF} \overset{d}{=} \frac{F_{1,N-L+1}(\delta_\beta)}{\beta_{N-L+2,L-1}} \quad (5)$$

$$\tilde{D}_{ACE} \overset{d}{=} \frac{F_{1,N-L+1}(\delta_\beta)}{1-\beta_{N-L+2,L-1}}, \quad (6)$$

where

$$\tilde{D}_{ACE} \triangleq \frac{D_{ACE}}{(1-D_{ACE})}, \quad (7)$$

and

$$\tilde{\eta}_{ACE} \triangleq \frac{\eta_{ACE}}{1-\eta_{ACE}}. \quad (8)$$

Note the two component detectors are written equal in distribution ($\overset{d}{=}$) to a function of the same two dependent random variables, $F_{1,N-L+1}$ (noncentral F) and $\beta_{N-L+2,L-1}$ (central Beta), as well as a single parameter,

$$\delta_\beta^2 = a^2\beta_{N-L+2,L-1}(\mathbf{s}^T\hat{\mathbf{\Gamma}}^{-1}\mathbf{s}), \quad (9)$$

often called the loss factor. This factor is related to SINR by way of the terms $a^2(\mathbf{s}^T\hat{\mathbf{\Gamma}}^{-1}\mathbf{s})$ in (9).

From (4) we can explicitly write

$$P_D = \Pr(D_{AMF} > \eta_{AMF}, D_{ACE} > \eta_{ACE}) =$$

$$\int_0^1 P_\beta d\beta \cdot \Pr(D_{AMF} > \eta_{AMF}|\beta, D_{ACE} > \eta_{ACE}), \quad (10)$$

in which we can substitute (5)-(8) to get

$$P_D = \Pr(D_{AMF} > \eta_{AMF}, D_{ACE} > \eta_{ACE}) =$$

$$\int_0^1 P_\beta d\beta \cdot \Pr[F_{1,N-L+1}(\delta_\beta) > \beta\eta_{AMF}|\beta,$$

$$F_{1,N-L+1}(\delta_\beta) > \eta_{\tilde{ACE}}(1-\beta)]. \quad (11)$$

The pdf of $\beta_{N-L+2,L-1}$ is given by

$$P_\beta = \frac{N!}{(N-L+1)!(L-2)!}\beta^{N-L+1}(1-\beta)^{L-2} \quad (12)$$

for $0 \leq \beta \leq 1$. It is worth mentioning that many of these expressions became accessible as the result of Kelly's comprehensive manuscripts, in this case [10] with Forsythe.

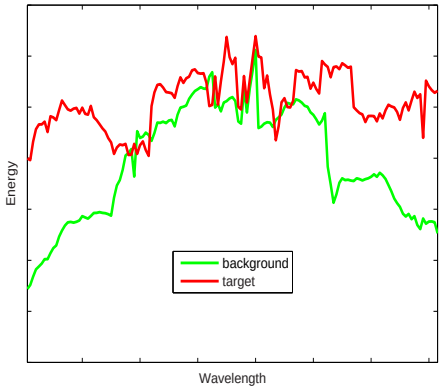

Fig. 3. Spectral profile of roof target and background.

5. A MODIFIED APPROACH

HSI is frequently employed in the detection of sub-pixel targets, or for targets whose spatial shape is not well-defined. Such difficult targets may have low SINR but good spectral contrast, despite their lack of morphological structure. This is depicted in figure 3. In this case, the ACE will be a more effective discriminator and it makes sense to apply this detector as the first stage in a two-stage algorithm. That way, as many of the background pixels will be discarded as possible, leaving a smaller number of candidate target pixels for which the AMF will be computed. This reduces processing cost. Conversely, a target may be set in a background of very similar material (including camouflage or other concealment), where it offers acceptable SINR but a low spectral contrast – the shape of the spectral signature of the target is similar to that of the background. This is depicted in figure 4. The AMF is well-suited for this scenario and as such should be computed as the first stage of a two-stage cascade. Pre-processing to evaluate spectral angle and SINR for a given target against the current background can be a guiding light in deciding which stage to put first.

The extreme case is when the target has a low SINR and minimal spectral contrast; this is truly challenging for HSI sensors.

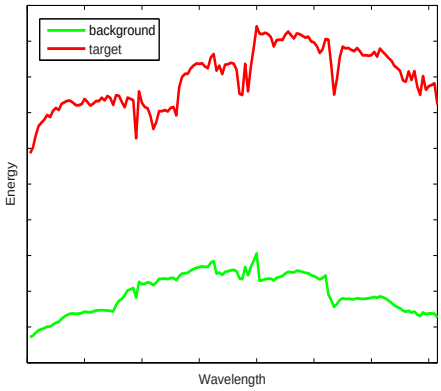

Fig. 4. Spectral profile of terrestrial target and background.

6. RESULTS

While theoretical ROC expressions and Monte Carlo simulations are important for evaluating expected performance of any detection scheme, in this paper we are interested in applying our modified two-stage approach to real-world hyperspectral data in order to make an initial evaluation of its utility in HSI detection. Sample support and dimensionality, among other things, are key differences between many radar applications and hyperspectral target detection – thus some of the novelty in applying this two-stage approach to HSI. Moreover, robust performance evaluation of HSI detection algorithms is challenging due to the limitations imposed by the limited amount of target data – typically less than 10^2 target pixels exist in a data set of 10^5 background pixels. As a result, the establishment of accurate ROC curves is quite difficult. Indeed, it is well known that as a rule of thumb the minimum number of N samples used to estimate a probability P should be at least 10/P, or better yet 100/P [11].

Hyperspectral image data from the 1998 low altitude deployment of the AVIRIS [12] sensor were used to evaluate the original and modified two-stage detection approaches. The AVIRIS sensor samples 224 contiguous spectral bands in the visible/NIR/SWIR from 400 nm - 2500 nm in wavelength. Once channels with poor spectral responses are removed, high attenuation due to atmospheric factors such as water vapor, there are $L = 143$ bands spaced at 10 nm on average. As a result of a lower than normal flight altitude, the particular AVIRIS data cube used has a spatial resolution of approximately two meters. The scene is from Moffett Field, an old Naval air station on the southern end of San Francisco bay near Sunnyvale, California. The scene is spectrally diverse and includes many different objects such as runways, dirt roads, paved roads, buildings, a variety of foliage, and various man-made materials. This is reflectance data, meaning that it has been atmospherically corrected

from its native radiance measurement space (using ATREM [13]). Such correction is a common pre-processing step that allows algorithm developers to exploit existing spectral libraries. Figure 5 shows an RGB color image (R=640 nm, G=550 nm, B=460 nm) of the Moffett scene.

Fig. 5. RGB image of AVIRIS scene: Moffett Field, CA.

In this scene the target is a non-metallic roof material on top of four buildings in the lower-left quadrant of the image. Figure 6 shows the spectral angle (in degrees) of all pixels in the image, color-coded so that red indicates a larger angle between the pixel vector and the mean vector of the background. Most all of the image is dark in color, and this dark (blue) represents the lack of spectral distinction that most of the pixels in the scene have with the background mean. This leads us to hypothesize that the ACE might be a good choice for the first stage of a cascade in detecting this target. Figure 7 shows the SINR of all pixels, in dB, where red (bright) is a high value and blue (dark) is a low value. Aside from the salt water ponds at the top of the image, most pixels in the scene have a small SINR value – including our targets. This suggests that the AMF would likely not eliminate many background pixels during a first stage.

Indeed, this turns out to be the case for modest threshold values. Figures 8 and 9 show thresholded images for 7° spectral angle and 0.5 dB SINR, respectively. Further examples for other targets will be presented at the workshop.

7. DISCUSSION

In this paper, we have discussed the application of a two-stage adaptive detector for hyperspectral imaging. The standard ASB applies the AMF to all samples and then the ACE

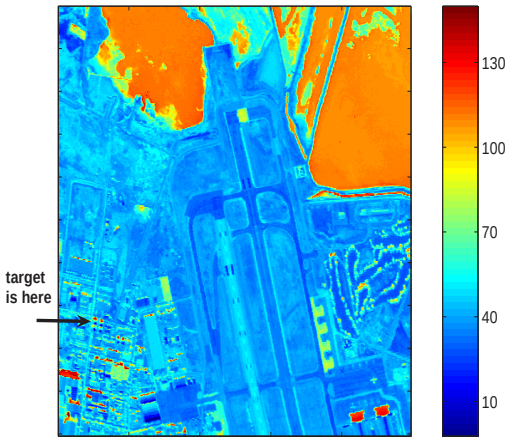

Fig. 6. Spectral angle, in degrees, for Moffett scene.

to those that pass AMF thresholding. We hypothesized that the reverse order is sometimes better-suited to hyperspectral targets, and indeed, our initial results show this to be the case for a number of targets. This reverse order approach was shown to perform better than the original cascade configuration for a few different targets in this initial evaluation. Obviously, this investigation is only a starting point; however, it presents a novel approach for HSI and opens the door for future work. Other studies will directly compare empirical results with theoretical performance bounds, and look into how the nature of the interference (i.e. physical background type: forest, desert, ocean) lends itself to homogeneity and consistency of results.

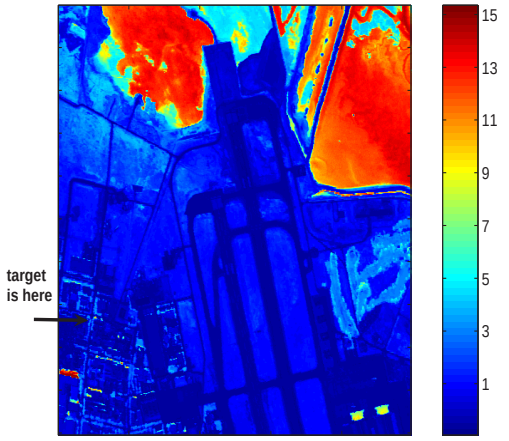

Fig. 7. SINR, in dB, for each pixel in Moffett scene.

8. REFERENCES

[1] I.S. Reed, J.D. Mallett, and L.E. Brennan, "Rapid Convergence Rate in Adaptive Arrays," *IEEE Trans. Aerospace and Electronic Systems*, vol. 10, pp. 853–863, 1974.

[2] E.J. Kelly, "An adaptive detection algorithm," in *IEEE Trans. Aerospace and Electronic Systems*, vol. 22, pp. 115–127, 1986.

[3] D. Kreithen and A. Steinhardt, "Target detection in post-STAP undernulled clutter," in *Proc. 29th Asilomar Conf. Signals, Systems, Comput.*, vol. 2, Nov. 1995, pp. 1203–1207.

[4] F.C. Robey, D.R. Fuhrmann, E.J. Kelly, and R. Nitzberg, "A CFAR adaptive matched filter detector," in *IEEE Trans. Aerospace and Electronic Systems*, vol. 28, pp. 208–216, 1992.

[5] L.L. Scharf and L.T. McWhorter, "Adaptive matched subspace detectors and adaptive coherence," in *IEEE Asilomar Conf. on Signals and Systems*, Pacific Grove, CA, 1996.

[6] D. Kreithen, C.F. Pearson, and C.D. Richmond, "Adaptive Sidelobe Blanker: a novel method of performance evaluation and threshold setting in the presence of inhomogeneous clutter," in *Proc. 32nd Asilomar Conf. Signals, Systems, Comput.*, vol. 1, Nov. 1998, pp. 528–532.

[7] C.D. Richmond, "Statistics of adaptive nulling and the use of the generalized eigenrelation for modeling inhomogeneities in adaptive processing," *IEEE Trans. Signal Processing*, vol. 48, no. 5, pp. 1263–1273, 2000.

[8] G. Shaw and D. Manolakis, "Signal processing for hyperspectral image exploitation," *IEEE Signal Processing Magazine*, vol. 19, no. 1, pp. 12–16, 2002.

[9] C.D. Richmond, "Performance of the adaptive sidelobe blanker detection algorithm in homogeneous environments," *IEEE Trans. Signal Processing*, vol. 48, no. 5, pp. 1235–1247, 2000.

[10] E.J. Kelly and K. Forsythe, "Adaptive detection and parameter estimation for multidimensional signal models," in *MIT Lincoln Laboratory Technical Report 848*, Lexington, MA, 1989.

[11] S.M. Kay, *Fundamentals of Statistical Signal Processing*, Prentice Hall, Englewood Cliffs, 1998.

[12] G. Vane, "First Results from the Airborne Visible/Infrared Imaging Spectrometer (AVIRIS)," in *JPL Publication 87-38/15*, NASA Jet Propulsion Laboratory, US, 1987.

[13] CSES/CIRES, *Atmospheric Removal Program (ATREM) Users Guide*, Ver. 3.0 ed. Boulder, CO: Center for the Study of Earth From Space (CSES) Cooperative Institute for Research in Environmental Sciences (CIRES), Univ. Colorado, 1997.

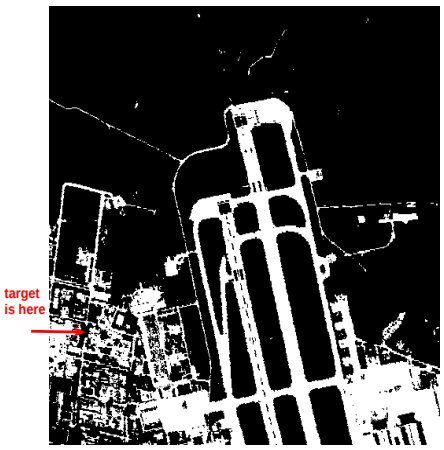

Fig. 8. Pixels exceeding modest power (length) threshold.

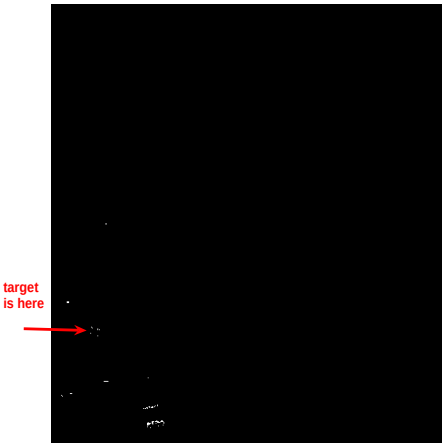

Fig. 9. Pixels exceeding modest spectral angle threshold.